AGU ADVANCING EARTH AND SPACE SCIENCE

Water Resources Research

RESEARCH ARTICLE

10.1029/2021WR029734

Key Points:

- An improved hydrodynamic module with regional parameterization to enhance sub-basin physical representation was developed
- Daily floods were modeled with relative error no more than 20% and *NSE* over 0.90 at selected stations
- Flood simulation without regional parameterization or reservoir regulation shows less satisfactory performance with lower *NSE*

Correspondence to:

Q. Tang,
tangqh@igsnrr.ac.cn

Citation:

Wang, J., Yun, X., Pokhrel, Y., Yamazaki, D., Zhao, Q., Chen, A., & Tang, Q. (2021). Modeling daily floods in the Lancang-Mekong River Basin using an improved hydrological-hydrodynamic model. *Water Resources Research*, *57*, e2021WR029734. https://doi.org/10.1029/2021WR029734

Received 3 FEB 2021
Accepted 21 JUL 2021

Modeling Daily Floods in the Lancang-Mekong River Basin Using an Improved Hydrological-Hydrodynamic Model

Jie Wang[1,2], Xiaobo Yun[1,2], Yadu Pokhrel[3], Dai Yamazaki[4], Qiudong Zhao[5,6], Aifang Chen[7], and Qiuhong Tang[1,2]

[1]Key Laboratory of Water Cycle and Related Land Surface Processes, Institute of Geographic Sciences and Natural Resources Research, Chinese Academy of Sciences, Beijing, China, [2]University of Chinese Academy of Sciences, Beijing, China, [3]Department of Civil and Environmental Engineering, Michigan State University, East Lansing, Michigan, USA, [4]Global Hydrological Prediction Center, Institute of Industrial Science, The University of Tokyo, Komaba, Japan, [5]Key Laboratory of Ecohydrology of Inland River Basin, Northwest Institute of Eco-Environment and Resources, Chinese Academy of Science, Lanzhou, China, [6]State Key Laboratory of Cryospheric Science, Northwest Institute of Eco-Environment and Resources, Chinese Academic of Sciences, Lanzhou, China, [7]School of Environmental Science and Engineering, Southern University of Science and Technology, Shenzhen, China

Abstract Daily floods including event, characteristic, extreme and inundation in the Lancang-Mekong River Basin (LMRB), crucial for flood projection and forecasting, have not been adequately modeled. An improved hydrological-hydrodynamic model (VIC and CaMa-Flood) considering regional parameterization was developed to simulate the flood dynamics over the basin from 1967 to 2015. The flood elements were extracted from daily time series and evaluated at both local and regional scales using the data collected from in-situ observations and remote sensing. The results show that the daily discharge and water level are both well simulated at selected stations with relative error (*RE*) less than 10% and Nash-Sutcliffe efficiency coefficient (*NSE*) over 0.90. Half of the flood events have *NSE* exceeding 0.76. The peak time and flood volume are well reproduced while both peak discharge and water level are slightly underestimated. The results tend to worsen when the characteristics of flood events are extended to annual extremes. These extremes are generally underestimated with *NSE* less than 0.5 but *RE* is within 20%. The simulated rainy season inundation area generally agrees with observations from remote sensing, with about 86.8% inundation occurrence frequency captured within the model capacity. Ignoring the regional parameterization and reservoir regulation can both deteriorate flood simulation performance at the local scale, resulting in lower *NSE*. Specifically, systematically higher water levels and up to 27% overestimation of peak discharge are found when ignoring regional parameterization, while ignoring reservoir regulation would cause up to 23% overestimation for flood extremes. It is expected that these findings would contribute to the regional flood forecasting and flood management.

1. Introduction

Lancang-Mekong River, one of the important transboundary rivers in the world, originates from Qinghai-Tibet Plateau and finally flows into the South China Sea through six riparian countries. Benefiting from the abundant water resources and annual flood pulse, the basin of the river (i.e., Lancang-Mekong River Basin, LMRB) breeds the largest wetland (Tonle Sap Lake, TSL) in Southeast Asia (Hoang et al., 2019), the third largest delta in the world (i.e., Mekong Delta, MDA) and the world's second richest basin in biodiversity (Anthony et al., 2015). A unique flow reversal between the TSL and Mekong River, developed by the seasonal flood pulse, brings timely water and nutrient-rich sediments to the TSL, supporting the TSL as the world's largest and most productive freshwater fishery (Pokhrel, Shin, et al., 2018). Such flow reversal and flood pulse in the Mekong River also provide water and nutrients for flood-recession agriculture in the MDA, which contributes to 90% of the Vietnam's rice production and makes this country the second most important rice exporters (Anthony et al., 2015; Pokhrel, Shin, et al., 2018). Nevertheless, the flood pulse makes the basin a flood-prone zone with the world highest flood-induced mortalities, especially for Mekong River Basin (MRB, excluding the Lancang River Basin in China) (e.g., Chen et al., 2020; Hu et al., 2018), where large floodplains are flooded annually during the flood season (Hoang et al., 2019). Moreover, this basin has experienced climate change, population increase, sea level rise, and intensified anthropogenic activities (e.g., dam construction) over the last decades (e.g., Hoang et al., 2019; Triet et al., 2020; Wang et al., 2017). It is expected that these threats will continuously challenge this basin, which can potentially lead to more frequent floods and thus greater flood risk in the future (e.g., Pokhrel, Burbano, et al., 2018). It is therefore crucial to better understand the changing flood dynamics of the basin.

Numerous methods have been used to study floods in the LMRB, for example, in-situ observation (e.g., Delgado et al., 2010), remote sensing (e.g., Boergens et al., 2019), and model simulation (e.g., Pokhrel, Shin, et al., 2018). However, the in-situ observations on the one hand are scarce and difficult to access in the riparian countries or organizations, especially for discharge data, even though the water level data have become relatively abundant from public websites in recent years. On the other hand, only limited information for floods can be revealed across a spatial scale because of the uneven distribution and low density of stations in the basin. Due to the cloud cover during rainy days (e.g., Ji et al., 2018), dense vegetation (e.g., Shin et al., 2020), and satellite repeat cycle (e.g., Boergens et al., 2019), remote sensing data from optical sensors (e.g., Landsat) or Radar (e.g., Sentinel) either underestimates flooded areas or entirely misses the flood events. Often, areas that are flooded are even excluded because of the limitations in water body identification algorithms or quality in remote sensing images (e.g., Lu et al., 2016). Moreover, both in-situ observation and remote sensing can only provide data within the observation period. This means flood forecasting and its historical reconstruction are essentially impossible by directly using these methods. Model simulations can fill these gaps by providing basin-wide discharges and water levels at the local scale, and spatially explicit inundation patterns at the regional scale. In-situ observation and remote sensing data can be used for model calibration and validation, where the missing values in the data are allowed and have less impact on the final results.

Traditionally, the hydrological models with different processes (i.e., infiltration, runoff, and flow routing) considered are used to model floods over large domains, such as XinAnJiang model (XAJ, Zhao et al., 1980), Variably Infiltration Capacity model (VIC, Liang et al., 1994), Distributed Biosphere-Hydrological model (DBH, Tang, 2006). Good performances of river discharge can be provided by these models, but these are still not ideal tools to study floods because discharge alone does not provide a complete understanding of flood dynamics, especially for the low-lying regions like MDA in the lower MRB. It is crucial to simulate water levels and inundation patterns using a hydrodynamic module where the backwater effect and channel bifurcation can be included (Yamazaki, Sato, et al., 2014). This hydrodynamic module explicitly represents flood dynamics by solving different forms of Saint-Venant equations, such as the kinematic wave that cannot account for backwater effect (e.g., Wu et al., 2014), diffusive wave (e.g., Yamazaki et al., 2011), and local-inertial wave (e.g., Yamazaki et al., 2013). The spatial inundation map that truly reflects floods can therefore be easily derived and compared with remote sensing data directly and conveniently. However, the hydrodynamic module is hard to change the total amount of water that routes to the outlet. Instead, it can only change the temporal distribution of discharge at the outlet with the given total water amount. This may greatly restrict the application of the global or regional runoff products, where these products might be inconsistent with the observations at a particular river basin or sub-basin. In this condition, instead of using the existing runoff products, using the runoffs produced by the hydrological model could be more appropriate, where the total water amount at the outlet can be adjusted to match the observed value by parameter calibration. Thus, an integrated hydrological-hydrodynamic model is more desirable when the accurate flood dynamic simulation is of interest.

Previous studies have demonstrated a large number of successful applications of the hydrological models in the LMRB (e.g., Lauri et al., 2014; Wang et al., 2016). In these studies, the daily or monthly discharge series were calibrated and compared with observations, and good results are achieved (e.g., Yun et al., 2020). Some studies also turned their views on floods, which treated the flood as the high value parts of the whole discharge series (e.g., Wang et al., 2017; Yun et al., 2020). The mean annual maximum flood and flood frequency derived from peaks-over-threshold approach based on multi-year or single-year scale were commonly analyzed in these studies. To include more hydrological elements (e.g., water level, inundation) and truly reflect the flood regime, a variety of hydrodynamic models were developed. For example, the advanced Catchment-Based Marco-scale Floodplain model (CaMa-Flood) developed by Yamazaki et al. (2011). Based on these hydrodynamic models, with the help of runoff provided by hydrological model, research was extended to simulate daily water level series, monthly and seasonal inundations (e.g., Pokhrel, Shin, et al., 2018; Shin et al., 2020). Moreover, analyses for particular flood event and annual maximum inundation area were also conducted (e.g., Try et al., 2018, 2020). The model performances in these studies are good not only for discharge, but also for water level and inundation map.

However, few studies have investigated the model capacity to simulate floods over the entire basin, especially through an integrated hydrological hydrodynamic model. Floods including event, characteristic, and extreme for discharge and water level at daily scale are not fully explored in these studies, so does the daily spatial inundation map. These are actually very important for flood projection using climate model and flood forecasting using meteorological numerical model. Further, the current hydrodynamic module has not considered the regional parameterization which could also be important for flood performance. Studies have indicated that the use of identical parameters for the entire basin is problematic (e.g., Mateo et al., 2014; Yamazaki et al., 2011), which can be attributed to the unique geomorphology and hydraulics of the basin and its sub-basins (Brinkerhoff et al., 2020). Accurate flood simulations thus require regional parameterization. Moreover, daily flood projection or forecasting often ignores reservoir regulation due to the difficulty in deriving the operation rules. In the LMRB, river discharge has been heavily affected by human activity after 2007 because of the constructions of a large number of dams in recent years (e.g., Lauri et al., 2012; Yun et al., 2020), which also has impacts on flood simulation without considering the reservoir regulation in the hydrodynamic module. Therefore, it is crucial to investigate this impact on flood performance.

In this study, our goal is to simulate the daily floods using the improved hydrological-hydrodynamic model (i.e., VIC and CaMa-Flood, the scheme refers to Lu et al., 2016 or Wei et al., 2020) that considers a regional parameterization in the hydrodynamic module. The flood event, characteristic, extreme and inundation map were extracted from the improved model and compared with the collected observed daily discharge, water level and remote sensing image. The impacts of using the basin-wide identical parameters in the hydrodynamic module (i.e., basin-wide parameterization) and without considering reservoir regulation scheme (i.e., ignoring reservoir regulation) on flood simulation were also separately discussed. This study can improve our ability to simulate floods, benefit the modeling community to advance the flood monitoring and forecasting capabilities, and help with managing flood risk.

2. Data and Methods

2.1. Model Description

The VIC model was used to provide daily surface and subsurface runoffs. It is a physically based large-scale model (Liang et al., 1994, 1996), which considers vegetation and topography at sub-grid and calculates energy and water budgets at daily or sub-daily scale. Snow melt and frozen soil physical processes are both considered, hence it is suitable for the application in the LMRB (Figure 1). With prescribed soil, vegetation, snow band data, and meteorological forcings (precipitation, temperature and wind speed), the model produces runoff among other surface hydrological fluxes. Usually, a river routing module called the Rout (Lohmann et al., 1996) or Routing Application for Parallel Computation of Discharge (RAPID; David et al., 2011) is integrated with VIC to provide discharge simulation, and has been widely used in regional and global studies (e.g., Lin et al., 2019; Zhao et al., 2019). Noting that the impact of glacier in the basin is very limited (Zhao et al., 2019). Thus, the VIC version 4.20d without considering the glacier module was used.

CaMa-Flood (Yamazaki et al., 2011, 2013), a global river hydrodynamic routing model, was used to route the runoff produced by VIC. It explicitly parameterizes the topography of sub-grid scale, and can simulate water level and flood inundation depth that are not typically simulated by river routing modules used in hydrological models such as VIC. A one-dimensional local inertial equation that can quantify the backwater effect was included in the model. Considering the divergent river channel systems in the lower basins, a bifurcation scheme was implemented in the CaMa-Flood model by Yamazaki, Sato, et al. (2014). A global width database for large rivers (Yamazaki, O'Loughlin, et al., 2014) was also coupled into the model to represent the river width, while the width of small river (i.e., less than 300 meters) and rive depth were calculated using the runoff related empirical equations (see Yamazaki et al., 2011). 500 meters spatial inundation

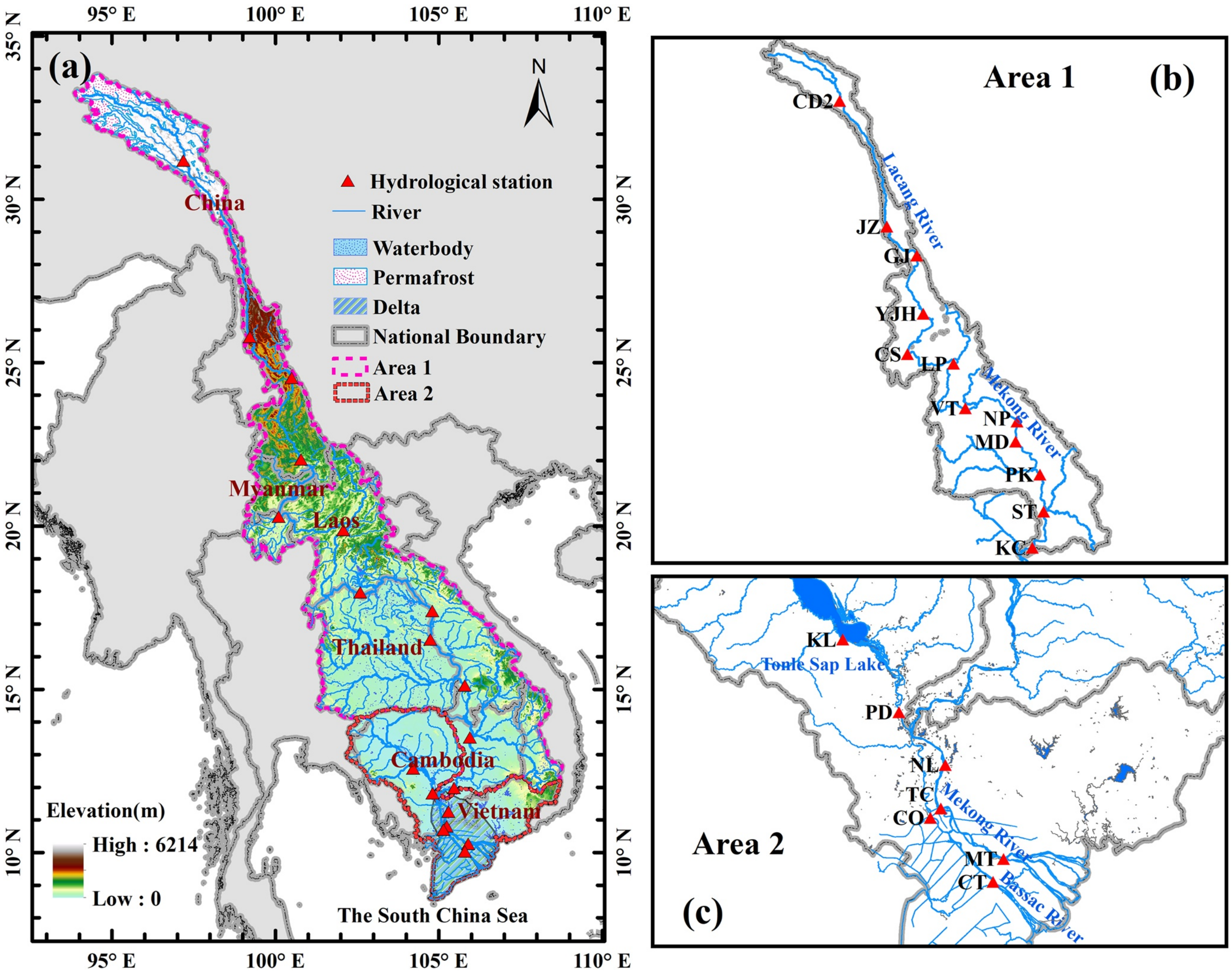

Figure 1. Overview of Lancang-Mekong River Basin (LMRB, a) and hydrological station distributions in partial areas (b, c). Area 1 (b) is mainly controlled by elevation with small portions affected by backwater, while Area 2 (c) is mainly controlled by water level with most areas affected by backwater.

map could be obtained using the water level data and Digital Elevation Model (DEM). In this study, the CaMa-Flood version 3.6.2 was used with the consideration of backwater effect and channel bifurcation.

2.2. Data Description

The daily meteorological data during 1961–2015 were obtained from CN05.1 (Wu & Gao, 2013), Asian Precipitation-Highly Resolved Observational Data Integration Toward the Evaluation of Water Resource (APHRODITE, Yatagai et al., 2009, 2012) and Princeton hydrological data set (Sheffield et al., 2006). The forcings in the Lancang River basin were provided by CN05.1, while APHRODITE provided precipitation and Princeton dataset provided temperature and wind speed in the MRB. These data were interpolated into 0.25° using the nearest neighbor method. Soil, vegetation and snow band data that are necessary for VIC model were obtained from the sources described in Zhao et al. (2019). Nineteen hydrological stations were considered mainly for calibration (Figure 1), some of which were selected for validation and analysis. Daily discharge and water level data for these stations were mainly collected from Henck et al. (2011), Mohammed et al. (2018), Annual Hydrological Reports of China, and Mekong River Commission (MRC). In addition, the daily 500m water body maps based on the Moderate Resolution Imaging Spectrometer (MODIS) during 2001–2015 were obtained from Ji et al. (2018). This dataset can reveal flood inundation, and hereafter is referred to as MODIS. To better simulate the flow reversal into TSL, a digital bathymetric

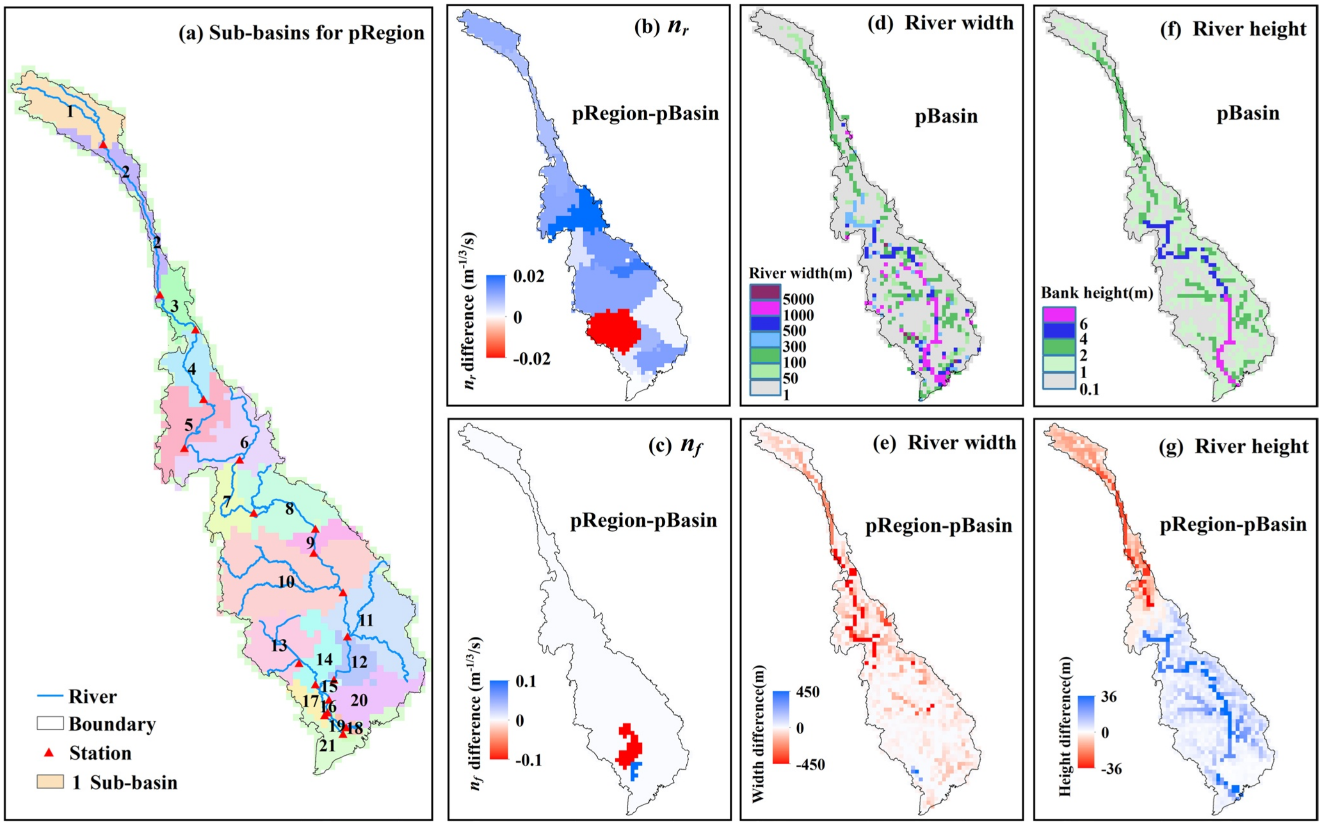

Figure 2. The sub-basins used for regional parameterization (pRegion, a), manning coefficients differences between the pRegion and basin-wide parameterization (pBasin) for river (n_r, b) and floodplain (n_f, c), river width (d) and depth (f) as well as their differences (e, g) between the pRegion and pBasin. The stations used for calibrations were also marked in (a). The n_r, n_f were finally determined as 0.022, 0.10 $m^{-1/3}/s$ for pBasin, respectively.

model of TSL collected from Kummu et al. (2014) was integrated into CaMa-Flood model mainly using the method described in Yamazaki et al. (2009).

2.3. Model Calibration

In CaMa-Flood only the basin-wide identical parameters can be calibrated, which may be not realistic due to the unique geomorphology and hydraulics (Brinkerhoff et al., 2020), Therefore, a regional parameterization calibration scheme, backward-compatible with basin-wide parameterization, was carried out in this study to enhance the physical representations of the hydrodynamic module in the sub-basins. This calibration scheme divides the basin into several independent sub-basins (Figure 2a), with each sub-basin characterized by identical parameters, and is detailed in Appendix A.

The spin-up period for both models was from 1961 to 1966, and the calibration and validation periods for VIC model were 1967–1991, 1992–2007, respectively. Period after 2007 were not selected because of the dam effect on the flow regimes (e.g., Hecht et al., 2019; Shin et al., 2020; Yun et al., 2020). The related main model parameters used for VIC can be found in Zhao et al. (2019) and Yun et al. (2020). The entire 1967–2007 period was used for the calibration of CaMa-Flood hydrodynamic parameters. Two manning coefficients for river and floodplain (i.e., n_r, n_f), and six coefficients for river width (i.e., power function constant and exponent WC, WP, and the minimum river width WIN) and river depth (i.e., power function constant and exponent HC, HP, and minimum river depth HMIN) empirical equations were used. The final calibrated manning coefficients, river width and depth for both regional and basin-wide parameterizations are illustrated in Figures 2b–2g.

Table 1
Daily Assessments for Discharge and Water Level

Station	Period	Discharge			Water level		
		NSE	RE	R	NSE	RE	R
CS	1967–2005	0.92	−0.00	0.96	0.90	-	0.95
LP	1967–2007	0.94	0.02	0.97	0.96	-	0.98
VT	1967–2007	0.94	0.01	0.97	0.95	-	0.98
NP	1967–2007	0.91	−0.08	0.97	0.97	-	0.98
MD	1967–2007	0.93	−0.05	0.97	0.96	-	0.98
PK	1967–2007	0.94	−0.02	0.98	0.95	-	0.98
ST	1967–2007	0.92	−0.04	0.97	0.95	-	0.98
KC	1967–2002	0.91	−0.09	0.97	0.96	-	0.98
NL	1967–2002	0.95	0.05	0.98	0.95	-	0.97

Note. NSE, R and RE are Nash-Sutcliffe efficiency coefficient, Person correlation coefficient, relative error respectively.

2.4. Flood Extraction and Assessment

Following the method proposed by the Water Resources Council of the United States (USWRC, 1976), a series of events independent of each other were extracted from the daily discharge series (also see Lang et al., 1999). To filter the small fluctuation that is indeed not the flood, the flood events (i.e., flood discharge events) were selected by simply requiring that the maximum peak of the event exceeded the long-term average of the discharge. Each simulated flood event corresponding to the observed one was extracted using the same time series. This was also extended to water level time series (i.e., extracting flood water level events). Four time series could therefore be obtained for one flood event (i.e., simulated water level and discharge, observed water level and discharge). Four flood characteristics including peak discharge, peak water level, peak time, and flood volume for each flood event were used. The peak discharge (water level) was defined as the maximum discharge (water level) of this flood event, while the time the maximum discharge occurs was considered as the peak time. The total water amount for the flood event was defined as the flood volume. Annual extremes were also calculated to assess the model capacity in simulating flood extremes. Four indices including annual maximum flood peak (AMFP), annual maximum water level (AMWL) and annual maximum flood volumes in three days (AM3DV) and seven days (AM7DV) were selected. The AMFP (AMWL) for a given year was the maximum discharge (water level) of the selected year, and the AM3DV (AM7DV) for a given year was defined as the maximum cumulative discharge for three (seven) consecutive days of the selected year. Since less information was revealed for how depth of water could be identified by MODIS, to maximally match the MODIS water body, the floodplain was assumed to be inundated when the flood depth is higher than 0.1 meters, while the river channel was considered to be always inundated.

The indices used to evaluate flood event, characteristic and annual extreme are Nash-Sutcliffe efficiency coefficient (*NSE*), Person correlation coefficient (*R*) and relative error (*RE*) (e.g., Wang et al., 2016; Zhao et al., 2019). Since the MODIS data do not detect all the water bodies, the probability of detection (POD), based on Wu, Adler, et al. (2012), was adopted to estimate the model inundation simulation capacity. POD was defined as the ratio of simultaneous inundation occurrence frequency (i.e., the number of inundation days) occurred for both model and MODIS to the inundation occurrence frequency occurred for MODIS. Hydrological stations on the Mekong River in the Area 1 (Figure 1b) with long records were used for water level and discharge evaluation, where the stations in the Lancang River Basin were not used because of the short daily records collected and large numbers of missing value. The stations in the Area 2 (Figure 1c) excluding NL were not used due to the short discharge records. Two stations (CS and ST) located on the northern and southern part of the MRB were used to analyze the impacts of basin-wide parameterization and ignoring the reservoir regulation. The NL station located in the MDA, witnessing frequent flood backwatering between the TSL and Mekong River, was selected to calibrate the basin-wide identical parameters in the hydrodynamic module using the same runoff input as in the regional parameterization scheme. For inundation evaluation, only rainy seasons from May to November were considered. The base study period used to evaluate daily flood simulations for regional parameterization and discuss the impact of basin-wide parameterization was 1967–2007, which was extended to 2008–2015 to further discuss the impact of ignoring reservoir regulation.

3. Results

3.1. Model Validation

The performances for daily discharge and water level at selected stations are listed in Table 1, and some representative seasonal hydrographs are shown in Figure 3. It can be seen the *RE*s for discharge and water level of all listed stations are within the range of 10% (Table 1). Most stations underestimate the total discharge amount, especially in the middle and lower reaches of MRB (i.e., NP, MD, ..., KC). This may be caused by the precipitation underestimation in the APHRODITE data set (refer to Figure 4 in Lauri et al., 2014). The *NSE*s

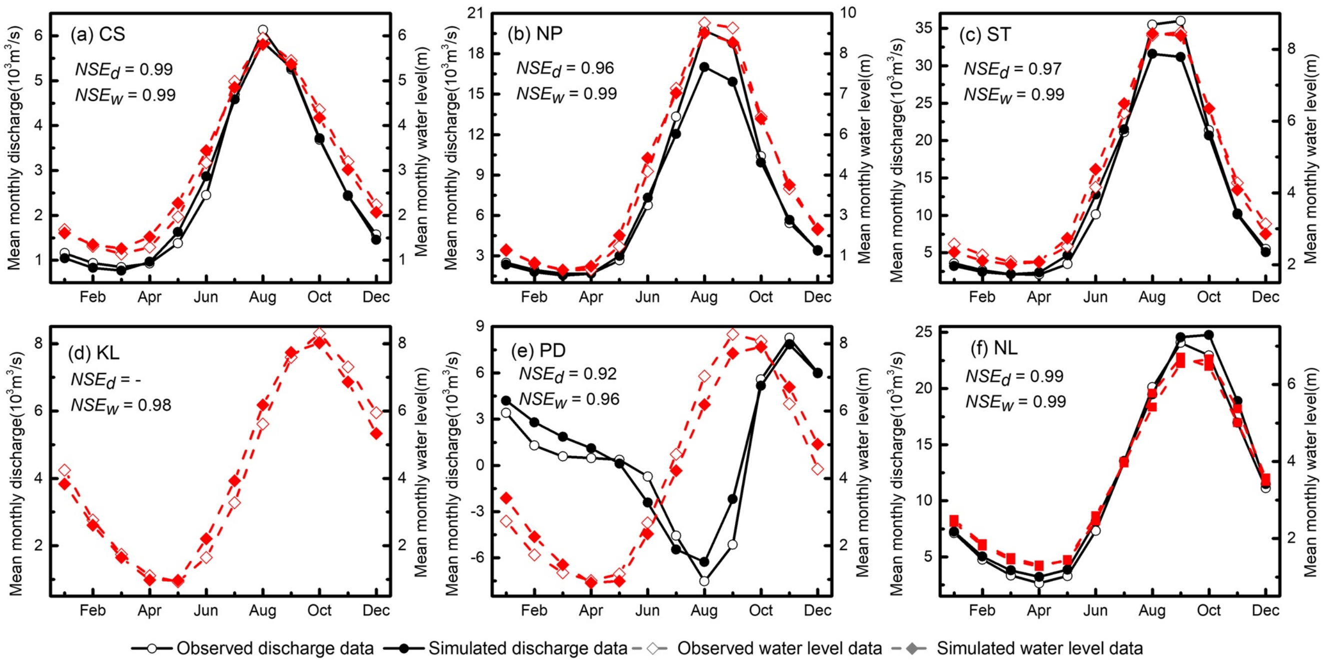

Figure 3. Observed and simulated seasonal discharge (solid line) and water level (dashed line) hydrographs for six selected stations. The subscripts "d" and "w" of *NSE* represent the average monthly discharge and water level, respectively. Stations illustrated in (a)–(c) and (d)–(f) are located in Area 1 and Area 2, respectively.

for both discharge and water level for these stations exceed 0.9. Similarly, the *R*s are all more than 0.95. The seasonal tendency and magnitude for discharge are well captured by the model in the upper MRB (i.e., CS, Figure 3a). However, the magnitudes during the period from July to September are underestimated in the middle and lower MRB (i.e., NP and ST, Figures 3b and 3c), even if the high *NSE*s are kept. The result tends to be much better when related to the MDA (i.e., NL, Figure 3f). Though slightly smaller *NSE* is obtained for the controlling station of the TSL (i.e., PD, Figure 3e), the tendency and magnitude are still simulated well, indicating the inverse flow into the TSL is well detected. In addition, the seasonal hydrographs for water level are performed with satisfactory performances both in tendencies and magnitudes.

3.2. Flood Event

The relative indices for flood events extracted from daily discharge and water level series are listed in Table 2. Four flood events at selected stations with *NSE* larger than 0.8 are shown in Figure 4. It can be found that the average number for detected flood events is decreased from four per year in the upstream stem (i.e., CS) to one in the downstream stem (i.e., NL), which could be attributed to the "planarization" of flood process caused by the relatively flat topography in the downstream areas. At selected stations, half of the flood discharge events have the *NSE* exceeding 0.76, and such proportion decreases to 45% when requiring *NSE* over 0.80. Except for CS, the *NSE*s for flood water level events tend to be slightly higher than those for discharge. The *R*s for half of the flood events at almost all the stations are larger than 0.95. Except for NP and KC, at least 51% of the flood discharge events exhibit an *RE* less than 10%. This is increased to 66% when flood water level events excluding CS are analyzed. The selected flood events shown in Figure 4 further reveal that the tendencies are well reproduced, whereas the magnitudes for peak discharge are mostly underestimated. Compared to the flood discharge event, the simulated flood water level event matches the observed one with a much smaller deviation.

3.3. Flood Characteristic

The flood characteristics including peak discharge, peak water level, peak time and flood volume for each flood event were extracted and their assessment indices are illustrated in Table 3. Their comparisons between

10.1029/2021WR029734

Table 2
Summary of Performances for Flood Event Simulation

station	Period	num	NSE_m	RE_m	R_m	P(NSE>0.8)	P(|RE|<0.1)	P(R>0.9)
CS	1967–2005	154	0.76(0.64)	0.01(0.02)	0.95(0.94)	0.45(0.37)	0.58(0.50)	0.75(0.69)
LP	1967–2007	138	0.82(0.82)	0.03(0.00)	0.96(0.96)	0.55(0.57)	0.62(0.86)	0.82(0.73)
VT	1967–2007	134	0.81(0.81)	0.02(-0.01)	0.96(0.95)	0.51(0.57)	0.63(0.74)	0.72(0.68)
NP	1973–2007	96	0.86(0.92)	−0.04(0.02)	0.98(0.98)	0.64(0.80)	0.43(0.77)	0.89(0.92)
MD	1967–2007	109	0.89(0.91)	−0.02(0.01)	0.97(0.98)	0.71(0.72)	0.56(0.79)	0.88(0.90)
PK	1967–2007	106	0.89(0.88)	−0.00(0.01)	0.97(0.97)	0.71(0.70)	0.62(0.66)	0.92(0.88)
ST	1967–2007	110	0.84(0.88)	−0.02(0.01)	0.96(0.97)	0.59(0.66)	0.51(0.78)	0.81(0.81)
KC	1967–2002	93	0.82(0.87)	−0.07(0.01)	0.97(0.98)	0.52(0.67)	0.45(0.72)	0.85(0.91)
NL	1980–2002	25	0.94(0.97)	0.07(0.03)	0.99(0.99)	0.88(0.96)	0.64(0.84)	1.00(1.00)

Note. “num” means the numbers of flood event. The subscript m for NSE, RE and R represents the median value for all the extracted flood events. P (NSE>0.8) means the percent satisfying the condition that NSE > 0.8, same as RE and R. Values outside the brackets refer to discharges, while those in brackets refer to the water level.

the observation and simulation at three stations are shown in Figure 5. The *NSE*s for peak discharge at all the stations excluding KC are larger than 0.70. Almost all the stations underestimate the peak discharge with the range from −3% to −20%, especially in the middle and lower MRBs (i.e., from NP to KC). The *R*s for most of these stations exceed 0.90. Similar results can be found for peak water level, but with much better overall performance than peak discharge. The simulated peak time matches well with the observed value

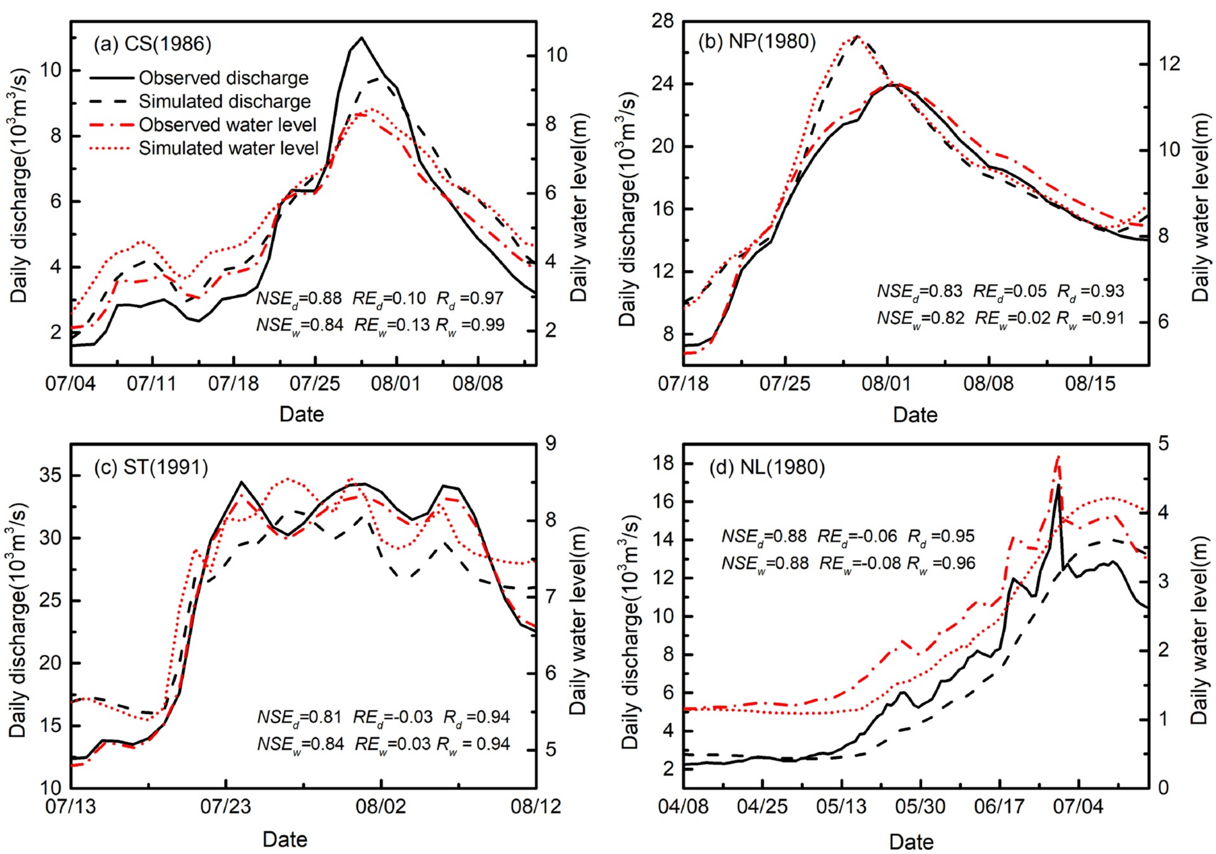

Figure 4. Observed and simulated discharge and water level hydrographs for the selected flood events at four stations. The flood event with Nash-Sutcliffe efficiency coefficient exceeding 0.8 for both water level and discharge and the smallest flood duration larger than 30 days was selected.

10.1029/2021WR029734

Table 3
Summary of Characteristics for Flood Events

	Peak discharge			Peak water level			Peak time			Flood volume		
Station	NSE	RE	R	NSE	RE	R	NSE	RE	R	NSE	RE	R
CS	0.74	−0.08	0.90	0.76	−0.04	0.88	0.99	−0.00	1.00	0.97	−0.00	0.99
LP	0.83	−0.03	0.92	0.86	−0.02	0.93	0.99	−0.00	0.99	0.98	0.02	0.99
VT	0.85	−0.04	0.93	0.84	−0.02	0.93	0.98	−0.01	0.99	0.98	0.01	0.99
NP	0.70	−0.11	0.89	0.86	−0.03	0.94	0.98	0.01	0.99	0.92	−0.07	0.98
MD	0.75	−0.12	0.93	0.85	−0.05	0.94	0.98	0.01	0.99	0.96	−0.05	0.99
PK	0.75	−0.14	0.94	0.82	−0.07	0.95	0.97	0.00	0.98	0.98	−0.02	0.99
ST	0.77	−0.10	0.90	0.72	0.02	0.91	0.96	−0.01	0.98	0.95	−0.04	0.98
KC	0.57	−0.20	0.93	0.83	−0.04	0.94	0.96	0.00	0.98	0.93	−0.10	0.98
NL	0.81	0.03	0.93	0.88	−0.00	0.94	0.58	0.05	0.92	0.92	0.06	0.97

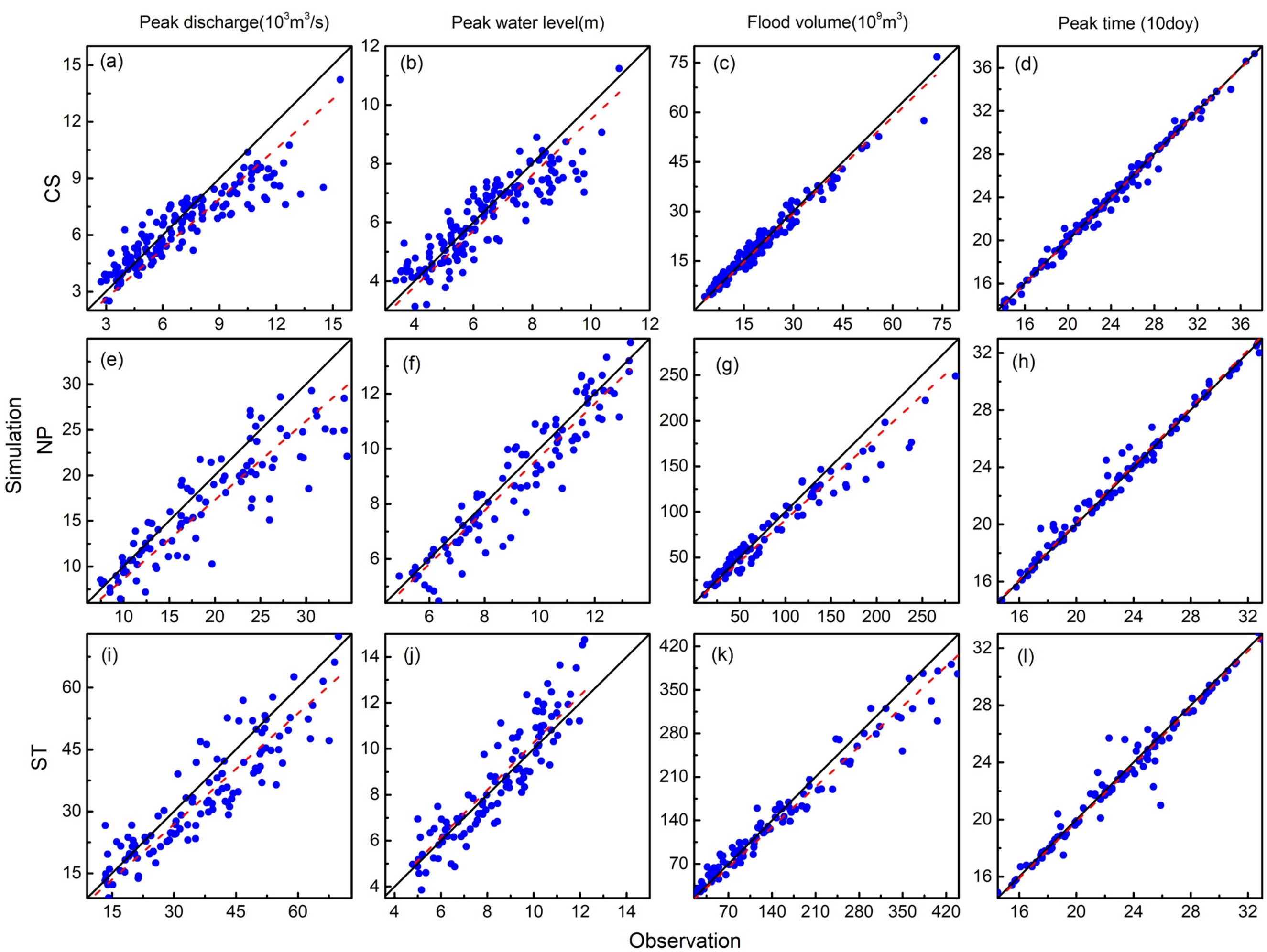

Figure 5. Observed and simulated flood characteristics comparisons at three selected stations. Panels from left to right are the peak discharge, peak water level, flood volume, and peak time occurring the peak discharge. Doy is the day of the year. The dash line is the curve fitting line between the observation and simulation.

10.1029/2021WR029734

Table 4
Summary of Performances for Annual Flood Extremes

	AMFP			AMWL			AM3DV			AM7DV		
Station	NSE	RE	R	NSE	RE	R	NSE	RE	R	NSE	RE	R
CS	−0.01	−0.17	0.76	0.29	−0.07	0.72	0.15	−0.15	0.78	0.30	−0.13	0.80
LP	0.45	−0.08	0.76	0.54	−0.04	0.80	0.53	−0.08	0.81	0.61	−0.08	0.86
VT	0.42	−0.09	0.79	0.39	−0.00	0.80	0.46	−0.09	0.81	0.50	−0.09	0.85
NP	0.06	−0.13	0.70	0.61	−0.02	0.84	0.05	−0.14	0.70	0.04	−0.14	0.70
MD	−0.18	−0.15	0.76	0.27	−0.07	0.81	−0.20	−0.15	0.75	−0.18	−0.16	0.75
PK	−0.08	−0.15	0.84	−0.00	−0.09	0.87	−0.05	−0.15	0.83	−0.02	−0.14	0.83
ST	0.19	−0.10	0.76	−0.41	0.06	0.81	0.18	−0.12	0.79	0.09	−0.14	0.81
KC	−1.28	−0.20	0.81	0.21	−0.03	0.83	−1.23	−0.20	0.81	−1.15	−0.20	0.82
NL	0.71	0.04	0.88	0.80	0.01	0.90	0.70	0.04	0.88	0.69	0.04	0.88

Note. AMFP and AMWL are separately the annual maximum discharge and annual maximum water level. AM3DV and M7DV are the annual maximum flood volumes in three days and seven days, respectively.

in the MRB with both *NSE* and *R* exceeding 0.95 and *RE* lower than 1%. Due to the backwater effect at NL, the peak time is overall overestimated and the *NSE* reduces to be lower than 0.60. Nevertheless, the flood volume at this station is well produced with both *NSE* and *R* larger than 0.92. The *NSE*s and *R*s for flood volume at stations in the MRB (i.e., CS, ..., KC) are all greater than 0.90, followed by less than 10% *RE*s being found. This is a little worse than those of peak time. Noting that the flood volumes at stations in the middle and lower MRB are also underestimated over 5%, but the extent is less than peak discharge. These results can be further confirmed in Figure 5. The peak time and flood volume between the simulation and observation at selected stations are basically close to the 1:1 line, meaning these two variables are well captured.

3.4. Flood Extreme

The AMFP, AMWL, AM3DV, AM7DV were assessed and are shown in Table 4. Figure 6 shows these annual flood extremes series varying with time at three selected stations. It can be found from Table 4 that these annual extremes are generally underestimated, especially in the middle and lower reaches of MRB as well as MDA. This could be largely attributed to the underestimation of the rainfall amount in APHRODITE data in these areas, where the precipitation plays a dominant role in modulating flood (e.g., Delgado et al., 2012). Such underestimations are also systematical for AMFP, AM3DV and AM7DV (Figure 6). The *NSE*s for these flood extremes are less than 0.5 or even negative. The simulation for AMWL is found to be slightly better with less underestimation. Compared to the results of flood characteristics (i.e., Table 3), those of the annual extremes are worse not only in terms of *NSE* but also in terms of *RE* and *R*, especially for the stations in the upper MRB (i.e., CS, LP). Nevertheless, the tendencies are relatively good with *R*s large than 0.7 at all the stations. Noting that the differences for AMFP, AM3DV and AM7DV continue to enlarge year by year since 1995 at NP station. This is likely caused by the underestimation of heavy storms, and warrants further investigation.

3.5. Flood Inundation

The spatial distribution of POD was obtained and is shown in Figure 7a. Two spatial inundation distribution maps during 2001 and 2002 (two severe flood years during 2001–2007), and their zoomed-in views are also illustrated in Figures 7b–7o. The results show that the most frequently flooded areas are mainly located in the TSL and MDA, followed by the Mun-Chi River Basin (MuRB) in eastern Thailand and Songkhram River Basin (SoRB) at upstream of the NP station (Figure 7a). The flooded areas detected by MODIS are well captured by the model, especially in the lower MRB, TSL and MDA. While the flooded areas in the MuRB and SoRB are basically captured, but with less spatial extent (Figure 7a). On average, 49.4% of the inundation occurrence frequency found by MODIS can be detected by the model. The undetected areas are

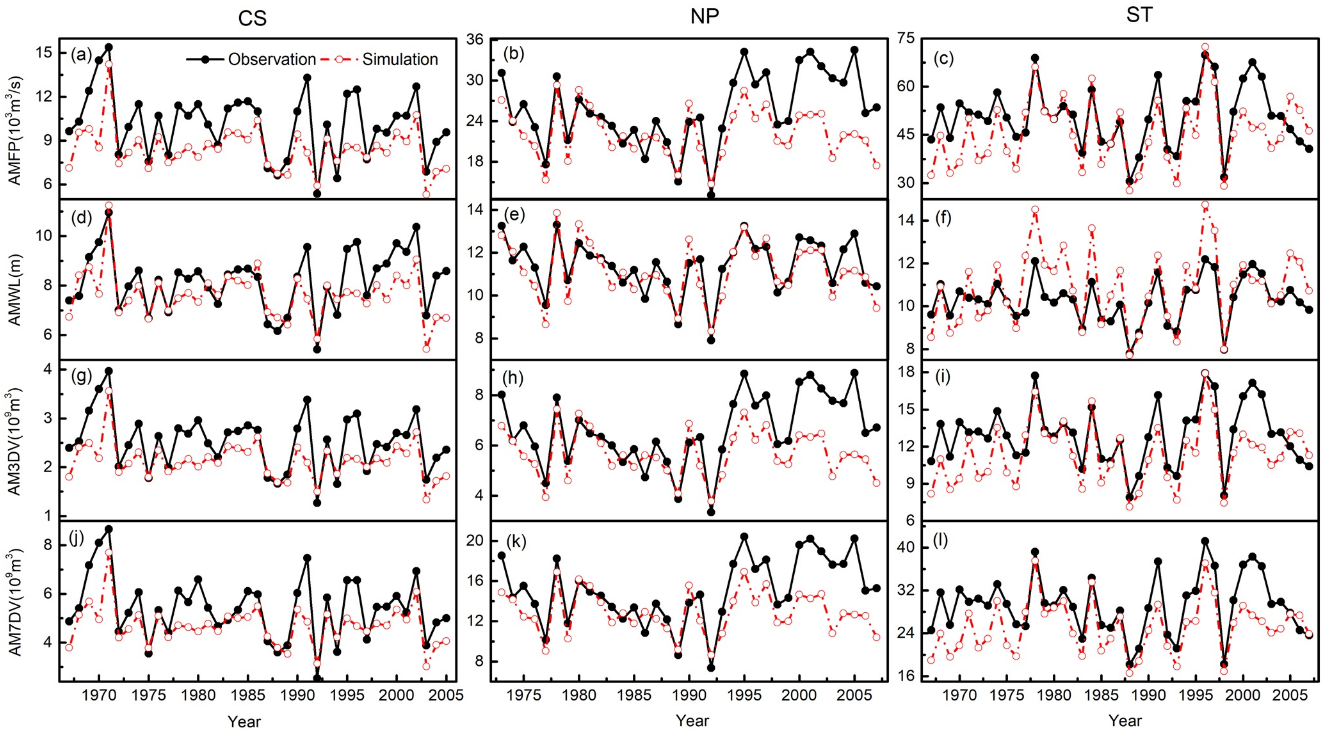

Figure 6. Comparisons of annual maximum flood peak, annual maximum water level and annual maximum flood volumes in three days and seven days between the observation and simulation at three stations. The left, middle and rights panels are for CS, NP, ST, respectively.

not only attributed to the inaccurate topography and ignoring tidal effect (Pokhrel, Shin, et al., 2018), but also attributed to the underestimation of water level (e.g., Figure 3b) and exclusion of small water bodies in the CaMa-Flood river map (e.g., Thailand parts in Figure 7a). If these factors are excluded (i.e., ignoring the zero-value of POD), then about 86.8% of the MODIS inundation occurrence frequency can be obtained using the model. This means the water body area detected by MODIS can be captured by the model at least once in all rainy seasons. The comparisons of the inundation maps further reveal that the simulated flood inundations perform well in the TSL, MDA, and MuRB, especially in the TSL (Figures 7b and 7c). The overestimation occurs in the MDA (Figures 7h, 7i, 7m and 7o), whereas the underestimation occurs in the MuRB (Figures 7f and 7k). This potentially suggests that the DEM with high accuracy or better model simulation capacity is required. Noting that the northwestern part of the area b-b in Figure 7b (also see Figures 7g and 7l), which is a wetland (Jun et al., 2014), is missed by MODIS (Figures 7d and 7i). This could indicate the water identification algorithm remains to be improved.

4. Discussion

4.1. Impact of Basin-Wide Parameterization

As the original CaMa-Flood uses the basin-wide parameterization (pBasin), comparisons between the two parameterizations (i.e., regional and basin-wide) are necessary. The results are shown in Figures 8 and 9. Compared to the results based on regional parameterization (pRegion), the mean annual water level at NL for pBasin is increased by 1.96 meters, while those at ST and CS are increased by 14.71 and 0.39 meters, respectively. The seasonal performances of discharge and water level at NL, CS, ST between the two parameterizations are similar (Figures 3 and 8). The daily discharge (water level) at NL for pBasin is also well produced with *NSE*, *RE* and *R* separately equaling to 0.95 (0.92), 0.01(0.00) and 0.97(0.96). Though the *NSE* of 0.93 for daily discharge at ST is much better than that of pRegion, the *NSE* for daily water level is reduced to 0.85. It turns to be much worse at CS, where *NSE*s for discharge and water level are separately decreased to 0.74 and 0.75 when compared with those of pRegion. The *R*s at CS are also reduced to 0.87 for both daily water level and discharge. For pBasin, the *NSE*s for half of the flood water level events at ST are over 0.62.

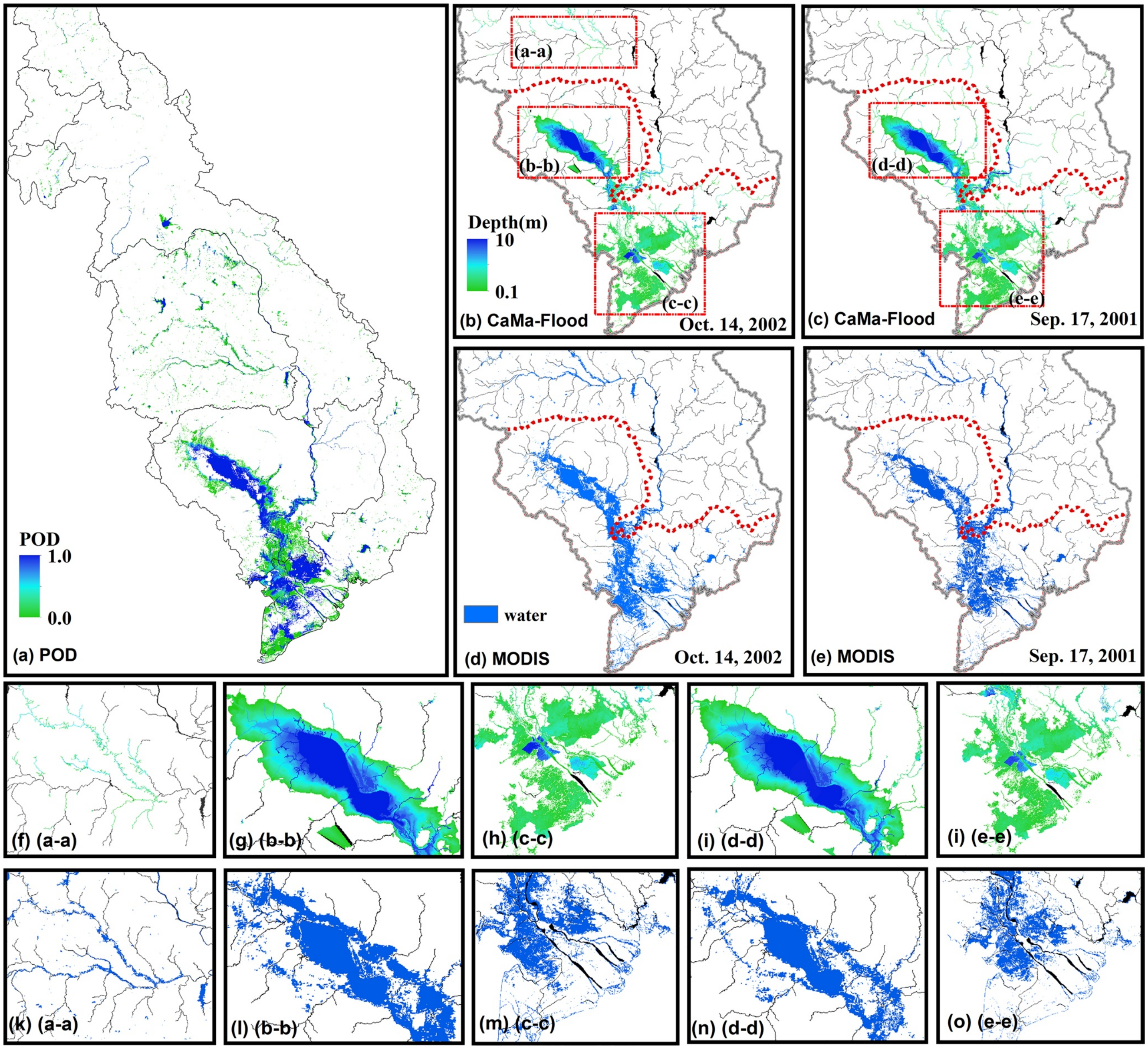

Figure 7. Spatial distribution of the probability of detection for rainy season inundation during 2001–2007 (a), two spatial inundation maps derived from CaMa-Flood (b, c) and MODIS (d, e), and their corresponding enlarged views (f–o). The dates with the maximum flooded area detected by Moderate Resolution Imaging Spectrometer (MODIS) in 2001 (d) and 2002 (e) were used for illustration. The black line as the background in (b–o) is the main river channel or reservoir, while the white background within the basin in (a–o) is the area with no inundation. The middle (f)–(i) and bottom (k–o) panels are for CaMa-Flood and MODIS, respectively.

The portion for flood water level events is decreased to 28% when *NSE* exceeding 0.8 is required. The median *NSE* for flood discharge (water level) events is even no more than 0.01 (−0.04) at CS for pBasin. No more than 7% (12%) of water level or discharge event have *NSE* (*R*) over 0.80 (0.90).

Also, compared with pRegion, the underestimation for peak discharge turns to be larger at ST, with *RE* increased from 10% to 16% (Table 3 and Figure 8e). The overestimation occurs at CS, with *RE* no less than 27% for peak discharge and no less than 14% for peak water level (Figures 8a and 8b). The other indices including *NSE* and *R* also show poorer performances, especially for CS. At CS, the *NSE* for peak discharge is decreased to 0.19, while that for peak water level is decreased to 0.34 (Table 3 and Figures 8a and 8b). Nevertheless, the peak time and flood volume show high consistence between the pRegion and pBasin (Table 3

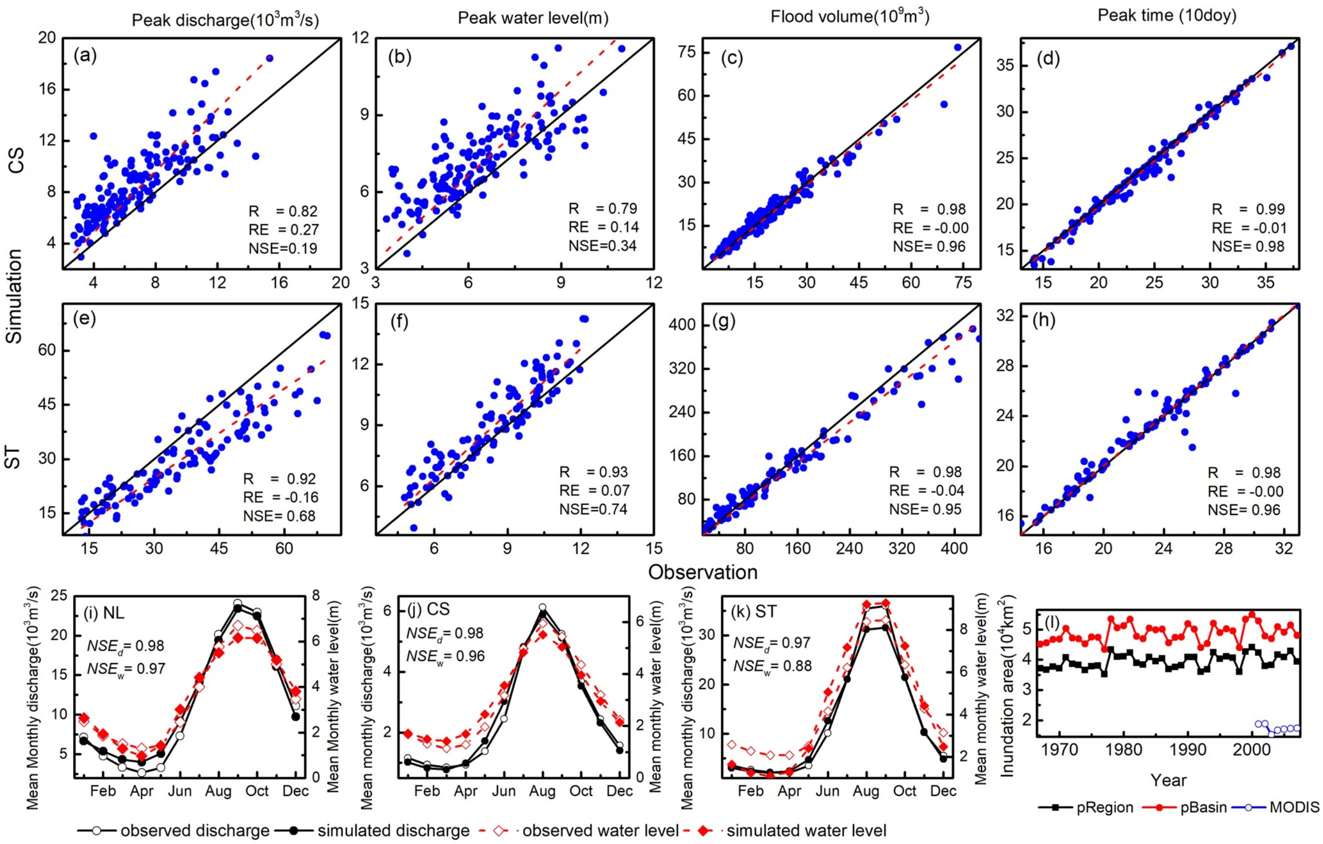

Figure 8. Comparisons of flood characteristics between the observation (bottom axis) and simulation (left axis) at two stations (a–h), the seasonal hydrographs (i–k) of discharge and water level, and annually average rainy season inundation area (l). Inundation areas for pRegion, pBasin and MODIS were all calculated. Here, river with the flood depth over the bank at least 0.1 m is added to the simulated inundation area.

and Figures 8c, 8d, 8g, 8h). Similar results can also be detected for flood extremes, where the underestimation for AMFP is larger than pRegion with *RE* increased to 17% at ST. The overestimations occur for AMFP, AMWL and AM3DV at CS with *RE* being 16%, 7%, and 8%, respectively. The *NSE*s at ST and CS for AMFP and AMWL are all becoming negative. The flood inundation maps at two selected dates (Figures 9a and 9b) also capture the flood dynamics for pBasin when compared to MODIS (Figures 7c and 7e), but with more flooded areas near the lower MRB and MDA (Figures 9c and 9d). More water concentrates on the main river channels and tributaries of lower MRB, which exceeds the storage capacity of channels. Noting that the decrease of inundation depth occurs on the tributaries far from the main streams in the upper and middle MRB (Figures 9c and 9d), which can be attributed to the water in these areas to fulfill the concentrated water occurring in the lower basin. The total inundation area for pBasin increases by 22.6% during 2001–2007 when compared with pRegion (Figure 8l).

4.2. Impact of Ignoring the Reservoir Regulation

Many dams have been constructed in the last several decades and the river discharge began to be heavily affected after 2007 because of the reservoir regulation. Thus, the predictability of the model that is calibrated and validated in 1967–2007 was expected to be degraded after 2007. To address this issue, the flood simulation was extended to the period of 2008–2015 using the same model and regional parameterization in the hydrodynamic model as those during 1967–2007. The results are shown in Figure 10 and 11. Lower observed discharge in the rainy season and higher observed discharge in the dry season are found at CS (Figures 3a and 10i), while such result is not obvious at ST. The *NSE*s for both daily discharge and water level are low at CS with the values less than 0.23. The water level was also underestimated by 11%. Whereas the *NSE*s at ST for both daily water level and discharge are slightly decreased with both values being 0.89.

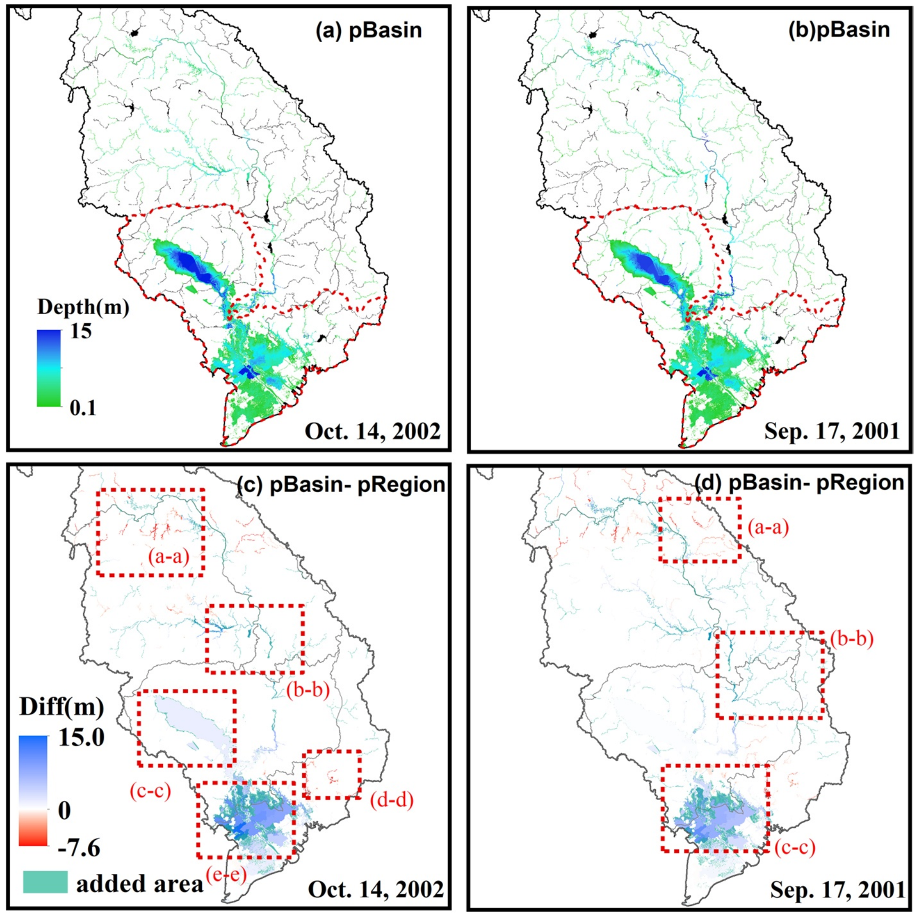

Figure 9. Spatial inundation maps (a, b) derived from CaMa-Flood with pBasin, and corresponding spatial inundation difference maps (c, d) between the pBasin and pRegion. Same dates with Figure 7 were selected.

Overestimations occur for discharge and water level with *RE*s separately being about 8% and 1%. Good correlation relation between the simulated and observed discharges (water levels) is preserved at ST. The median *NSE* value for the extracted flood discharge (water level) events is −0.23 (−1.28) at CS, while that is 0.76(0.77) at ST. Almost all the flood events at CS have *NSE* less than 0.80, whereas about 39% of those at ST have *NSE* over 0.80. This indicates that ignoring reservoir regulation deteriorates the flood event simulation with different degrees.

The peak discharge at CS is overestimated while peak water level is underestimated, with both *NSE*s negative (Figures 10a and 10b), worse than those before 2008 (Table 3). At ST, the peak water level and peak discharge are performed slightly poorly, with both *RE*s less than 1% and *NSE*s over 0.60 (Figures 10e and 10f; Table 3). Flood volumes at both CS and ST are overestimated with *RE* up to 13% at CS (Figures 10c and 10g), whereas the corresponding *RE* value at CS during 1967–2007 is 0% (Table 3). The peak time at two stations is still well captured by the model (Table 3; Figures 10d and 10h). Compared with the results during 1967–2007, the impacts of ignoring reservoir regulation on annual extremes after 2007 are further worse. The overestimations at CS occur for AMFP (12%), AMWL (6%), AM3DV (17%), and AM7DV (23%), and *NSE*s for these variables are all less than −5. The overestimations also occur for ST but with all *RE*s less than 5%. The *R*s for these four variables at ST and CS are all decreased with the maximum value being 0.60 when compared with those during 1967–2007. The detection of flood inundation occurrence frequency is similar to that before 2008, with the mean POD of about 0.5 (Figure 11a). If the water body found by MODIS can be captured by the model at least once (i.e., within the model capacity), then about 85.9% of MODIS inundation occurrence frequency can be obtained using the model. Figure 11 also shows that the spatial inundation map is well captured by the model. For example, the flood inundation in the MuRB, which is

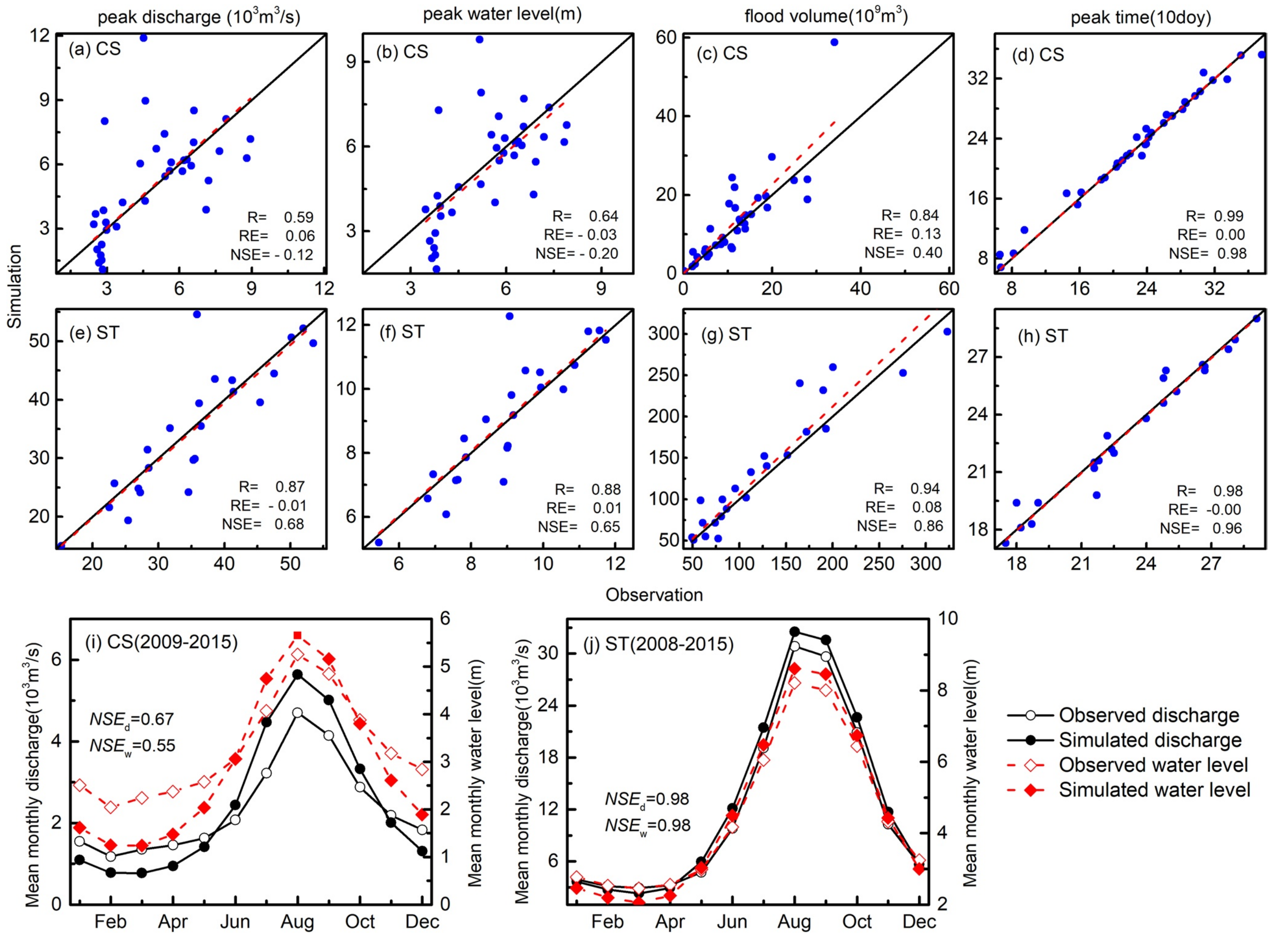

Figure 10. Comparisons between the observed and simulated flood characteristics (a–h) and seasonal hydrographs of discharge and water level (i–j) during 2008–2015. The points numbers used for CS and ST are 35 and 23, respectively.

thought to be one of the catastrophic floods in Thailand. Note the flooded area occurring upstream of the reservoir (Figures 11h and 11m), which is underestimated by the model due to the lack of the reservoir regulation scheme.

4.3. Uncertainties and Limitations

Precipitation is one of the main drivers of flood, and can be regarded as the most important uncertainty source of the meteorological inputs, as discussed in previous studies (e.g., Chen et al., 2018; Lauri et al., 2014; Wang et al., 2016). To decrease the impact caused by precipitation uncertainty, the APHRODITE which has been proved to be one of the best precipitation datasets in MRB hydrological practice (e.g., Lauri et al., 2014; Try et al., 2020) was used. Since the available observed precipitation data are relatively scarce in the LMRB (Lauri et al., 2012, 2014; Yatagai et al., 2009) and station distribution is uneven (Wang et al., 2016), spatiotemporally interpolated precipitation dataset applied in flood simulation requiring high accuracy can be still affected. Consequently, it may contribute substantially to the underestimated discharge during August and September in the middle and lower MRB (Figures 3b and 3c) and the underestimations for flood characteristics and flood extremes (Tables 3 and 4). This indicates the improvement of precipitation quality is essential (e.g., sharing with more observed precipitation data). The topography can also be another important uncertainty source in flood simulation and has been specifically explored (e.g., Hawker et al., 2018; Minderhoud et al., 2019), which suggests a DEM with high accuracy is necessary. In this study, the backwater effects generally exist in the MDA and areas surrounding the TSL, which are partly regulated

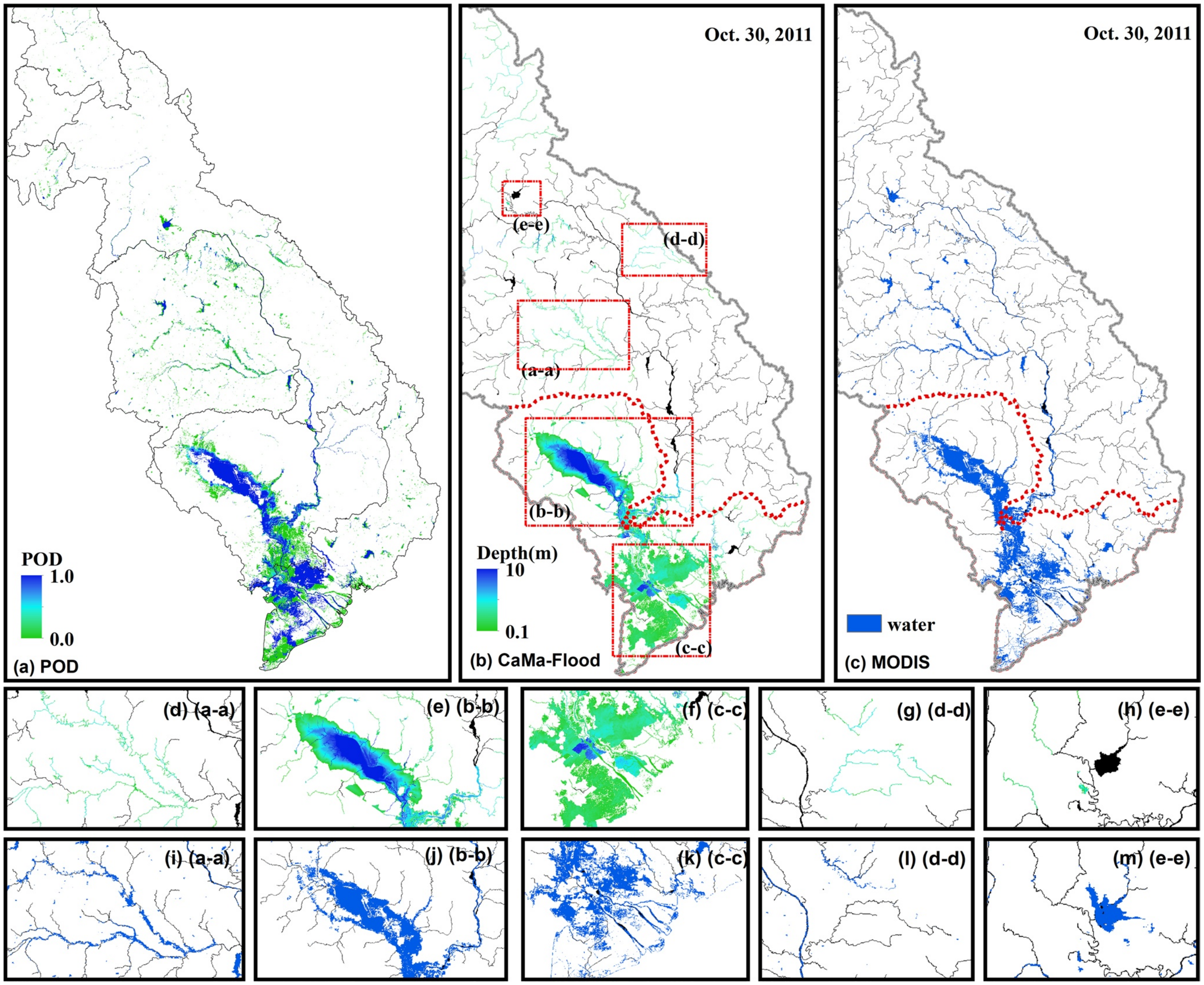

Figure 11. Spatial distribution of the rainy season flood inundation probability of detection during 2008–2015 (a), spatial inundation maps derived from CaMa-Flood (b) and Moderate Resolution Imaging Spectrometer (MODIS) (c) on October 30, 2011, and their corresponding enlarged views (d–m). The date with the maximum flooded area detected by MODIS from 2008 to 2015 was used for illustration. The middle (d–h) and bottom (i–m) panels are for CaMa-Flood and MODIS, respectively.

by the topography. Due to the potential error exists in topography, many flooded areas detected by the MODIS image are not captured by the model, especially in the MuRB and northern MDA. The inundation in the southern MDA is also found to be larger than that in MODIS (Figures 7b and 7c). Model parameterization and model structure also comprise the uncertainty sources. Because the basin experiences complex hydro-climate conditions including the frozen soil and snow in the Lancang River Basin and reversed flow in the TSL, calibration at as many representative stations as possible is necessary to enhance the physical representation at the sub-basin level. Further, though some flood characteristics at ST remain similar when the reservoir regulation is ignored, these flood characteristics at CS are not well produced (Figure 10). Also, high water levels and larger flooded areas can be introduced if the basin-wide identical parameters were used (Section 4.1).

Because of the intensified human activities (urbanization, deforestation) (e.g., Huong & Pathirana, 2013; Kim et al., 2019), the land surface becomes relatively impervious, potentially causing a high flood peak. This kind of landcover change is not considered in our model and is worthy of consideration in future studies. Further, there has been a recent increase in dam construction in the LMRB to meet the growing

10.1029/2021WR029734

energy needs (Pokhrel, Burbano, et al., 2018; Wang et al., 2017), which is suggested to have altered the flood pulse in the main stem (Shin et al., 2020; Yun et al., 2020, Section 4.2). Hence, it is important to consider reservoir regulation in the model for a more realistic simulation of flood dynamics. Shin et al. (2020) and Dang et al. (2020) have attempted to simulate the dam operation processes, but an extended evaluation on floods or developing new reservoir schemes is needed. Noting that flood inundation caused by small floods was not assessed due to the topographic issues and limited affected areas, which can be further studied. Because of the impacts of clouds and vegetations, uncertainties in water body classification methods, and quality in remote sensing images, only POD was used as an indicator of flood inundation. A more comprehensive evaluation of flood inundation dynamics could be achieved by using Landsat, Sentinel (e.g., Shin et al., 2020) or satellite altimetry (e.g., Boergens et al., 2019) datasets.

5. Summary and Conclusion

This study modeled the daily floods including event, characteristic, and annual extreme as well as flood inundation in the LMRB using an improved hydrological-hydrodynamic model that considers the regional parameterization in the hydrodynamic model. The impacts of ignoring regional parameterization and missing reservoir regulation were also discussed.

The daily discharge and water level are well simulated with their *RE*s within 10% and *NSE*s over 0.90 at selected stations. Their seasonal magnitudes and tendencies are also reproduced by the model reasonably well. The flood event numbers decrease from four per year in the upper MRB to one in the lower basin. In most MRB stations, half of the flood events have *NSE* exceeding 0.76, where the performance for water level tends to be slightly better.

The results of flood characteristics reveal that the *NSE*s for peak discharge and peak water level are larger than 0.74 at most stations. Both variables are underestimated with over 10% *RE* reached by peak discharge. The simulated peak time and flood volume match well with the observed values, with less than 10% *RE* found. However, the results tend to be worse when annual extremes are analyzed. The AMFP, AMWL, AM3DV and AM7DV are generally underestimated with *NSE* less than 0.5 or even negative. The *RE*s for AMFP and AMWL is worse but still within 20%.

The flooded areas frequently occurred are mainly distributed in the TSL, MDA, and MuRB. On average 49.4% of the MODIS daily water occurrence frequency can be captured by the model, and this proportion can be raised to 86.8% when MODIS water occurrence can be detected at least once in all rainy seasons. The spatial inundation map can be primarily captured by the model with overestimation in the MDA and underestimation in the MuRB.

Compared with those of regional parameterization, systematically higher water levels can be introduced for basin-wide parameterization. Though similar seasonal tendencies and magnitudes for both discharge and water level are found, their daily performances tend to be poorer. The simulations for flood event, characteristic, and extreme are therefore mainly deteriorated with lower *NSE*. Overestimation is found for peak discharge (27%) and peak water level (14%), while the peak time and flood volume are less impacted. The total inundation area is increased by 22.6% during 2001–2007 for basin-wide parameterization.

Compared with the results before 2008, the daily discharge and water level during 2008–2015 have lower *NSE*s at both the upper and lower stations, with daily water level underestimated by 11% reached at the upper station. The flood event, characteristic, and extreme are primarily deteriorated, with their *NSE*s less than −5 and *RE*s up to 23% found at the upper station. The simulation for peak time is less impacted and similar POD can be found if the reservoir regulation scheme is not considered in the model.

Appendix A: Regional Parameterization Calibration

This calibration scheme divides the basin into several independent sub-basins based on the locations of the hydrological station and flow direction, with each sub-basin characterized by identical parameters and corresponding to a station as much as possible. Noting that not all the water flow distributed on the left and right sides of MDA directly flow into the river reaches owning the available in-situ stations (Figure 1c, near the estuaries), two areas located at the two sides were added as the sub-basins, hence 21 sub-basins in total were identified for this calibration scheme (Figure 2a). The remaining grids located on the boundary of the basin, not belonging to any of the above sub-basins, were allocated to the last sub-basin (i.e., sub-basin 21). Such allocation did not have much impact on the results. If the regional parameterization calibration scheme was used to calibrate the basin-wide identical parameters, then the entire basin was treated as a whole.

The hierarchical upstream-downstream calibration strategy used by Wu, Kimball, et al. (2012) was adopted to calibrate the model parameters from upstream to downstream for both VIC and CaMa-Flood with the regional parameterization calibration scheme (i.e., improved CaMa-Flood). The calibration processes were done manually by trial and error, with the direction of the parameter adjustment following the parameter sensitivity description in studies such as Nijssen et al. (1997), Zhang et al. (2014) and Yamazaki et al. (2011). Two steps were designed to conduct the calibration: The first step is the calibration in the Area 1 with little backwater effect (Figure 1), followed by that in the Area 2 with backwater effect (i.e., the second step).

In the Area 1 with 12 sub-basins, to decrease the time consuming of running CaMa-Flood and avoid the impact of parameters for CaMa-Flood on discharge, the Rout integrated with VIC was used to calibrate the parameters for VIC, with the aim to minimize the difference between the simulated and observed seasonal discharge hydrographs. Then the runoff was input to the improved CaMa-Flood to calibrate the parameters for CaMa-Flood, with the aim to minimize the difference between the simulated and observed seasonal water level hydrographs while also ensure that the performance of seasonal discharge hydrographs did not drop too much. Usually, the seasonal discharge hydrographs can be well kept when minimizing the water level difference.

While in the Area 2, the parameters separately for VIC and improved CaMa-Flood in the nine sub-basins were calibrated mutually due to the backwater effect and river channel bifurcation in the TSL and MDA. A preferred aim to minimize the difference between the simulated and observed seasonal water level hydrographs while also improve the performance of seasonal discharge hydrographs as much as possible was used for both VIC and CaMa-Flood calibrations. The initial parameters for VIC in these nine sub-basins used those of sub-basin controlled by KC (Figure 1b). Then the model parameters for improved CaMa-Flood were calibrated at nine sub-basins one by one. This process was repeated until marginal improvement (or relatively good result) was achieved. After this, the VIC model parameters were adjusted at these sub-basins using the same strategy as the improved CaMa-Flood. Such calibrations for the improved CaMa-Flood and VIC as described above were repeated until relatively good results at the calibrated stations were found.

There were two issues should be noted: One was the calibration in the Area 2 could lead to the decline in the water level performance in the Area 1 because of the lower boundary change in the local inertial equation used in CaMa-Flood. When this happened, the parameters for CaMa-Flood should be re-calibrated slightly for the sub-basins near the affected station to keep a relatively steady boundary. The other issue was for height datum and DEM error, to make a comparable water level, the simulated water level in this research was reduced by the difference of the mean long-term simulated and observed water levels following Shin et al. (2020).

Data Availability Statement

The CaMa-Flood can be visited at http://hydro.iis.u-tokyo.ac.jp/~yamadai/cama-flood/, and VIC model source codes can be available from https://vic.readthedocs.io/en/master/. Parts of the discharge data and water level data are from the MRC website (https://portal.mrcmekong.org/, last visited on March 15, 2020). The postprocessing MODIS water body data from Ji et al. (2018) can be available at http://data.ess.tsinghua.edu.cn/modis_500_2001_2016_waterbody.html. The APHRODITE data can be downloaded from http://aphrodite.st.hirosaki-u.ac.jp/download/, and the Princeton hydrological dataset is available at http://hydrology.princeton.edu/data/pgf/v3/0.25deg/daily/.

Acknowledgments

This work was supported by the National Natural Science Foundation of China (41730645), the Strategic Priority Research Program of Chinese Academy of Sciences (XDA20060402), the International Partnership Program of Chinese Academy of Sciences (131A11KYSB20180034). Yadu Pokhrel received support from the National Science Foundation (CAREER Award; grant #:1752729). Aifang Chen received support from the China Postdoctoral Science Foundation (2021M691403). Thanks are due to Dr. Siao Sun for her comments and editorial advice.

References

Anthony, E. J., Brunier, G., Besset, M., Goichot, M., Dussouillez, P., & Nguyen, V. L. (2015). Linking rapid erosion of the Mekong River delta to human activities. *Scientific Reports*, *5*, 14745. https://doi.org/10.1038/srep14745

Boergens, E., Dettmering, D., & Seitz, F. (2019). Observing water level extremes in the Mekong River Basin: The benefit of long-repeat orbit missions in a multi-mission satellite altimetry approach. *Journal of Hydrology*, *570*, 463–472. https://doi.org/10.1016/j.jhydrol.2018.12.041

Brinkerhoff, C. B., Gleason, C. J., Feng, D., & Lin, P. (2020). Constraining remote river discharge estimation using reach-scale geomorphology. *Water Resources Research*, *56*(11), e2020WR027949. https://doi.org/10.1029/2020wr027949

Chen, A., Chen, D., & Azorin-Molina, C. (2018). Assessing reliability of precipitation data over the Mekong River Basin: A comparison of ground-based, satellite, and reanalysis datasets. *International Journal of Climatology*, *38*(11), 4314–4334. https://doi.org/10.1002/joc.5670

Chen, A., Giese, M., & Chen, D. (2020). Flood impact on Mainland Southeast Asia between 1985 and 2018—The role of tropical cyclones. *Journal of Flood Risk Management*, *13*(2), e12598. https://doi.org/10.1111/jfr3.12598

Dang, T. D., Vu, D. T., Chowdhury, A. K., & Galelli, S. (2020). A software package for the representation and optimization of water reservoir operations in the VIC hydrologic model. *Environmental Modelling & Software*, *126*, 104673. https://doi.org/10.1016/j.envsoft.2020.104673

David, C. H., Maidment, D. R., Niu, G. Y., Yang, Z. L., Habets, F., & Eijkhout, V. (2011). River network routing on the NHDPlus dataset. *Journal of Hydrometeorology*, *12*(5), 913–934. https://doi.org/10.1175/2011jhm1345.1

Delgado, J. M., Apel, H., & Merz, B. (2010). Flood trends and variability in the Mekong river. *Hydrology and Earth System Sciences*, *14*(3), 407–418. https://doi.org/10.5194/hess-14-407-2010

Delgado, J. M., Merz, B., & Apel, H. (2012). A climate-flood link for the lower Mekong River. *Hydrology and Earth System Sciences*, *16*(5), 1533–1541. https://doi.org/10.5194/hess-16-1533-2012

Hawker, L., Rougier, J., Neal, J., Bates, P., Archer, L., & Yamazaki, D. (2018). Implications of simulating global digital elevation models for flood inundation studies. *Water Resource Research*, *54*(10), 7910–7928. https://doi.org/10.1029/2018wr023279

Hecht, J. S., Lacombe, G., Arias, M. E., Dang, T. D., & Piman, T. (2019). Hydropower dams of the Mekong River basin: A review of their hydrological impacts. *Journal of Hydrology*, *568*, 285–300. https://doi.org/10.1016/j.jhydrol.2018.10.045

Henck, A. C., Huntington, K. W., Stone, J. O., Montgomery, D. R., & Hallet, B. (2011). Spatial controls on erosion in the Three Rivers Region, southeastern Tibet and southwestern China. *Earth and Planetary Science Letters*, *303*(1-2), 71–83. https://doi.org/10.1016/j.epsl.2010.12.038

Hoang, L. P., van Vliet, M. T., Kummu, M., Lauri, H., Koponen, J., Supit, I., et al. (2019). The Mekong's future flows under multiple drivers: How climate change, hydropower developments and irrigation expansions drive hydrological changes. *The Science of the Total Environment*, *649*, 601–609. https://doi.org/10.1016/j.scitotenv.2018.08.160

Hu, P., Zhang, Q., Shi, P., Chen, B., & Fang, J. (2018). Flood-induced mortality across the globe: Spatiotemporal pattern and influencing factors. *The Science of the Total Environment*, *643*, 171–182. https://doi.org/10.1016/j.scitotenv.2018.06.197

Huong, H. T. L., & Pathirana, A. (2013). Urbanization and climate change impacts on future urban flooding in Can Tho city, Vietnam. *Hydrology and Earth System Sciences*, *17*(1), 379–394. https://doi.org/10.5194/hess-17-379-2013

Ji, L., Gong, P., Wang, J., Shi, J., & Zhu, Z. (2018). Construction of the 500-m resolution daily global surface water change database (2001–2016). *Water Resource Research*, *54*(12), 10–270. https://doi.org/10.1029/2018wr023060

Jun, C., Ban, Y., & Li, S. (2014). China: Open access to earth land-cover map. *Nature*, *514*, 434. https://doi.org/10.1038/514434c

Kim, S., Sohn, H. G., Kim, M. K., & Lee, H. (2019). Analysis of the relationship among flood severity, precipitation, and deforestation in the Tonle Sap Lake Area, Cambodia using multi-sensor approach. *KSCE Journal of Civil Engineering*, *23*, 1330–1340. https://doi.org/10.1007/s12205-019-1061-7

Kummu, M., Tes, S., Yin, S., Adamson, P., Józsa, J., Koponen, J., et al. (2014). Water balance analysis for the Tonle Sap Lake–floodplain system. *Hydrological Processes*, *28*(4), 1722–1733. https://doi.org/10.1002/hyp.9718

Lang, M., Ouarda, T. B. M. J., & Bobée, B. (1999). Towards operational guidelines for over-threshold modeling. *Journal of Hydrology*, *225*(3–4), 103–117. https://doi.org/10.1016/s0022-1694(99)00167-5

Lauri, H., De Moel, H., Ward, P. J., Räsänen, T. A., Keskinen, M., & Kummu, M. (2012). Future changes in Mekong River hydrology: Impact of climate change and reservoir operation on discharge. *Hydrology and Earth System Sciences Discussions*, *16*, 4603–4619. https://doi.org/10.5194/hess-16-4603-2012

Lauri, H., Räsänen, T. A., & Kummu, M. (2014). Using reanalysis and remotely sensed temperature and precipitation data for hydrological modeling in monsoon climate: Mekong River case study. *Journal of Hydrometeorology*, *15*(4), 1532–1545. https://doi.org/10.1175/jhm-d-13-084.1

Liang, X., Lettenmaier, D. P., Wood, E. F., & Burges, S. J. (1994). A simple hydrologically based model of land surface water and energy fluxes for general circulation models. *Journal of Geophysical Research*, *99*(D7), 14415–14428. https://doi.org/10.1029/94jd00483

Liang, X., Wood, E. F., & Lettenmaier, D. P. (1996). Surface soil moisture parameterization of the VIC-2L model: Evaluation and modification. *Global and Planetary Change*, *13*(1–4), 195–206. https://doi.org/10.1016/0921-8181(95)00046-1

Lin, P., Pan, M., Beck, H. E., Yang, Y., Yamazaki, D., Frasson, R., et al. (2019). Global reconstruction of naturalized river flows at 2.94 million reaches. *Water Resources Research*, *55*(8), 6499–6516. https://doi.org/10.1029/2019wr025287

Lohmann, D., NOLTE-HOLUBE, R. A. L. P. H., & Raschke, E. (1996). A large-scale horizontal routing model to be coupled to land surface parametrization schemes. *Tellus A*, *48A*, 708–721. https://doi.org/10.3402/tellusa.v48i5.12200

Lu, X., Zhuang, Q., Liu, Y., Zhou, Y., & Aghakouchak, A. (2016). A large-scale methane model by incorporating the surface water transport. *Journal of Geophysical Research:Biogeosciences*, *121*(6), 1657–1674. https://doi.org/10.1002/2016jg003321

Mateo, C. M., Hanasaki, N., Komori, D., Tanaka, K., Kiguchi, M., Champathong, A., et al. (2014). Assessing the impacts of reservoir operation to floodplain inundation by combining hydrological, reservoir management, and hydrodynamic models. *Water Resources Research*, *50*(9), 7245–7266. https://doi.org/10.1002/2013wr014845

Minderhoud, P. S. J., Coumou, L., Erkens, G., Middelkoop, H., & Stouthamer, E. (2019). Mekong delta much lower than previously assumed in sea-level rise impact assessments. *Nature Communications*, *10*, 3847. https://doi.org/10.1038/s41467-019-11602-1

Mohammed, I. N., Bolten, J. D., Srinivasan, R., & Lakshmi, V. (2018). Satellite observations and modeling to understand the Lower Mekong River Basin streamflow variability. *Journal of Hydrology*, *564*, 559–573. https://doi.org/10.1016/j.jhydrol.2018.07.030

Nijssen, B., Lettenmaier, D. P., Liang, X., Wetzel, S. W., & Wood, E. F. (1997). Streamflow simulation for continental-scale river basins. *Water Resources Research*, *33*(4), 711–724. https://doi.org/10.1029/96wr03517

Pokhrel, Y., Burbano, M., Roush, J., Kang, H., Sridhar, V., & Hyndman, D. W. (2018). A review of the integrated effects of changing climate, land use, and dams on Mekong river hydrology. *Water*, *10*(3), 266. https://doi.org/10.3390/w10030266

Pokhrel, Y., Shin, S., Lin, Z., Yamazaki, D., & Qi, J. (2018). potential disruption of flood dynamics in the Lower Mekong River basin due to upstream flow regulation. *Scientific Reports*, *8*, 17767. https://doi.org/10.1038/s41598-018-35823-4

Sheffield, J., Goteti, G., & Wood, E. F. (2006). Development of a 50-year high-resolution global dataset of meteorological forcings for land surface modeling. *Journal of Climate*, *19*(13), 3088–3111. https://doi.org/10.1175/jcli3790.1

Shin, S., Pokhrel, Y., Yamazaki, D., Huang, X., Torbick, N., Qi, J., et al. (2020). High resolution modeling of river-floodplain-reservoir inundation dynamics in the Mekong River Basin. *Water Resources Research*, *56*(5), e2019WR026449. https://doi.org/10.1029/2019wr026449

Tang, Q. (2006). A distributed biosphere-hydrological model for continental scale river basins (Doctoral dissertation). Ph. D. thesis, University of Tokyo.

Triet, N. V. K., Dung, N. V., Hoang, L. P., Le Duy, N., Tran, D. D., Anh, T. T., et al. (2020). Future projections of flood dynamics in the Vietnamese Mekong Delta. *The Science of the Total Environment*, *742*, 140596. https://doi.org/10.1016/j.scitotenv.2020.140596

Try, S., Lee, G., Yu, W., Oeurng, C., & Jang, C. (2018). Large-scale flood-inundation modeling in the Mekong River basin. *Journal of Hydrologic Engineering*, *23*(7), 05018011. https://doi.org/10.1061/(asce)he.1943-5584.0001664

Try, S., Tanaka, S., Tanaka, K., Sayama, T., Oeurng, C., Uk, S., et al. (2020). Comparison of gridded precipitation datasets for rainfall-runoff and inundation modeling in the Mekong River Basin. *PloS One*, *15*(1), e0226814. https://doi.org/10.1371/journal.pone.0226814

USWRC. (1976). Guidelines for Determining Flood Flow Frequency (Vol. 17, p. 73). United States Water Resources Council, Bull.Hydrol. Comm.

Wang, W., Lu, H., Ruby Leung, L., Li, H. Y., Zhao, J., Tian, F., et al. (2017). Dam construction in Lancang-Mekong River basin could mitigate future flood risk from warming-induced intensified rainfall. *Geophysical Research Letters*, *44*(20), 10–378. https://doi.org/10.1002/2017gl075037

Wang, W., Lu, H., Yang, D., Sothea, K., Jiao, Y., Gao, B., et al. (2016). Modelling hydrologic processes in the Mekong River Basin using a distributed model driven by satellite precipitation and rain gauge observations. *PloS One*, *11*(3), e0152229. https://doi.org/10.1371/journal.pone.0152229

Wei, Z., He, X., Zhang, Y., Pan, M., Sheffield, J., Peng, L., et al. (2020). Identification of uncertainty sources in quasi-global discharge and inundation simulations using satellite-based precipitation products. *Journal of Hydrology*, *589*, 125180. https://doi.org/10.1016/j.jhydrol.2020.125180

Wu, H., Adler, R. F., Hong, Y., Tian, Y., & Policelli, F. (2012). Evaluation of global flood detection using satellite-based rainfall and a hydrologic model. *Journal of Hydrometeorology*, *13*(4), 1268–1284. https://doi.org/10.1175/jhm-d-11-087.1

Wu, H., Adler, R. F., Tian, Y., Huffman, G. J., Li, H., & Wang, J. (2014). Real-time global flood estimation using satellite-based precipitation and a coupled land surface and routing model. *Water Resources Research*, *50*(3), 2693–2717. https://doi.org/10.1002/2013wr014710

Wu, H., Kimball, J. S., Elsner, M. M., Mantua, N., Adler, R. F., & Stanford, J. (2012). Projected climate change impacts on the hydrology and temperature of Pacific Northwest rivers. *Water Resources Research*, *48*(11), W11530. https://doi.org/10.1029/2012wr012082

Wu, J., & Gao, X. J. (2013). A gridded daily observation dataset over China region and comparison with the other datasets. *Chinese Journal of Geophysics (in Chinese)*, *56*(4), 1102–1111.

Yamazaki, D., de Almeida, G. A., & Bates, P. D. (2013). Improving computational efficiency in global river models by implementing the local inertial flow equation and a vector-based river network map. *Water Resources Research*, *49*(11), 7221–7235. https://doi.org/10.1002/wrcr.20552

Yamazaki, D., Kanae, S., Kim, H., & Oki, T. (2011). A physically based description of floodplain inundation dynamics in a global river routing model. *Water Resources Research*, *47*(4), W04501. https://doi.org/10.1029/2010wr009726

Yamazaki, D., Oki, T., & Kanae, S. (2009). Deriving a global river network map and its sub-grid topographic characteristics from a fine-resolution flow direction map. *Hydrology and Earth System Sciences*, *13*(11), 2241–2251. https://doi.org/10.5194/hess-13-2241-2009

Yamazaki, D., O'Loughlin, F., Trigg, M. A., Miller, Z. F., Pavelsky, T. M., & Bates, P. D. (2014). Development of the global width database for large rivers. *Water Resources Research*, *50*(4), 3467–3480. https://doi.org/10.1002/2013wr014664

Yamazaki, D., Sato, T., Kanae, S., Hirabayashi, Y., & Bates, P. D. (2014). Regional flood dynamics in a bifurcating mega delta simulated in a global river model. *Geophysical Research Letters*, *41*(9), 3127–3135. https://doi.org/10.1002/2014gl059744

Yatagai, A., Arakawa, O., Kamiguchi, K., Kawamoto, H., Nodzu, M. I., & Hamada, A. (2009). A 44-year daily gridded precipitation dataset for Asia based on a dense network of rain gauges. *Sola*, *5*, 137–140. https://doi.org/10.2151/sola.2009-035

Yatagai, A., Kamiguchi, K., Arakawa, O., Hamada, A., Yasutomi, N., & Kitoh, A. (2012). APHRODITE: Constructing a long-term daily gridded precipitation dataset for Asia based on a dense network of rain gauges. *Bulletin of the American Meteorological Society*, *93*(9), 1401–1415. https://doi.org/10.1175/bams-d-11-00122.1

Yun, X., Tang, Q., Wang, J., Liu, X., Zhang, Y., Lu, H., et al. (2020). Impacts of climate change and reservoir operation on streamflow and flood characteristics in the Lancang-Mekong River Basin. *Journal of Hydrology*, *590*, 125472. https://doi.org/10.1016/j.jhydrol.2020.125472

Zhang, X. J., Tang, Q., Pan, M., & Tang, Y. (2014). A long-term land surface hydrologic fluxes and states dataset for China. *Journal of Hydrometeorology*, *15*(5), 2067–2084. https://doi.org/10.1175/jhm-d-13-0170.1

Zhao, Q., Ding, Y., Wang, J., Gao, H., Zhang, S., Zhao, C., et al. (2019). Projecting climate change impacts on hydrological processes on the Tibetan Plateau with model calibration against the glacier inventory data and observed streamflow. *Journal of Hydrology*, *573*, 60–81. https://doi.org/10.1016/j.jhydrol.2019.03.043

Zhao, R. J., Zhang, Y. L., Fang, L. R., Liu, X. R. & Zhang, Q. S. (1980). The Xinanjiang Model, Hydrological Forecasting Proceedings Oxford Symposium. IASH.